

Spin dynamics of the director state in frustrated hyperkagome systems

Henrik Jacobsen,^{1,2,3,4} Ovidiu Florea,⁵ Elsa Lhotel,⁵ Kim Lefmann,⁶ Oleg Petrenko,⁷ Chris S. Knee,^{8,9} Tilo Seydel,¹⁰ Paul F. Henry,^{11,12,8,4} Robert Bewley,¹¹ David Voneshen,^{11,13} Andrew Wildes,¹⁰ Gøran Nilsen,^{10,11} and Pascale P. Deen^{4,3}

¹*Paul Scherrer Institute, Laboratory for Neutron Scattering and Imaging, 5232 Villigen, Switzerland*

²*Department of Physics, Oxford University, Oxford, OX1 3PU, United Kingdom*

³*Nanoscience Center, Niels Bohr Institute, University of Copenhagen, 2100 Copenhagen Ø, Denmark*

⁴*European Spallation Source, Tunavägen 24, 223 63 Lund, Sweden*

⁵*Institut Néel, CNRS and Université Grenoble Alpes, 38000 Grenoble, France*

⁶*Nanoscience Center, Niels Bohr Institute, University of Copenhagen, 2100 Copenhagen Ø, Denmark*

⁷*Department of Physics, University of Warwick, Coventry, CV4 7AL, UK*

⁸*Department of Chemical and Biological Engineering,*

Chalmers University of Technology, Gothenburg SE 412 96, Sweden

⁹*ESAB AB, Lindholmsallén 9, Box 8004, SE-402 77, Gothenburg, Sweden*

¹⁰*Institute Laue-Langevin, 71 avenue des Martyrs, BP156, 38042 Grenoble Cedex 9, France*

¹¹*ISIS Facility, Rutherford Appleton Laboratory, Chilton, Didcot, OX11 0QX, Oxfordshire, UK*

¹²*Uppsala University, Department of Chemistry, Ångström Laboratory, Box 538, SE-751 21 Uppsala, Sweden*

¹³*Department of Physics, Royal Holloway University of London, Egham, TW20 0EX, UK.*

We present an experimental study of the magnetic structure and dynamics of two frustrated hyperkagome compounds, $\text{Gd}_3\text{Ga}_5\text{O}_{12}$ and $\text{Gd}_3\text{Al}_5\text{O}_{12}$. It has previously been shown that $\text{Gd}_3\text{Ga}_5\text{O}_{12}$ exhibits long-range correlations of multipolar directors, that are formed from antiferromagnetic spins on loops of ten ions. Using neutron diffraction and Reverse Monte Carlo simulations we prove the existence of similar magnetic correlations in $\text{Gd}_3\text{Al}_5\text{O}_{12}$, showing the ubiquity of these complex structures in frustrated hyperkagome materials. Using inelastic neutron scattering we shed further light on the director state and the associated low-lying magnetic excitations. In addition we have measured quasielastic dynamics that show evidence of spin diffusion. Finally, we present AC susceptibility measurements on both $\text{Gd}_3\text{Ga}_5\text{O}_{12}$ and $\text{Gd}_3\text{Al}_5\text{O}_{12}$, revealing a large difference in the low frequency dynamics between the two otherwise similar compounds.

I. INTRODUCTION

Emergence is the phenomenon of collective behavior that does not depend solely on the individual parts of a system, but rather through their interactions. This effect often results in novel and diverse states of matter. For example, in the field of magnetic frustration, emergent phenomena have been gracefully demonstrated by the observation of magnetic monopoles emerging in spin ice materials¹⁻⁵.

A further example is the director state uncovered in the geometrically frustrated garnet, $\text{Gd}_3\text{Ga}_5\text{O}_{12}$ (GGG)⁶. The Gd^{3+} ions in GGG form two interpenetrating hyperkagome lattices. In these structures, the resultant moment on connected loops of ten ions form a nematic director state at low temperatures⁶. Fig. 1 illustrates three such ten-ion loops. Taking the position of each director as the atom at the center of the ten-ion loop (illustrated in black), the directors also form a hyperkagome structure.

The directors in GGG are reminiscent of the emergent cluster state in the geometrically frustrated spinel ZnCr_2O_4 ⁷, where groups of six spins self-organise into decoupled antiferromagnetic (AF) loops, also known as director protectorates.

It has been suggested that such directors are inherent in geometrically frustrated systems, and that they provide an organising principle in which emergent clusters

form out of a manifold of ground states with the low temperature dynamics governed by the director state.

In $\text{Gd}_3\text{Ga}_5\text{O}_{12}$ the director state originates from the interplay between near-neighbor AF interactions and local xy anisotropy⁶. The directors are highly anisotropic and align along their local z -axis. The alignment of all the directors along their local z axis leads to long range correlations, in contrast to the decoupled directors in ZnCr_2O_4 . The observed magnetic excitations in GGG range from the peV to the meV scale⁸⁻¹³, and the ten-ion loops seem to be central to understanding these dynamics in GGG^{8,13}.

In this paper we delve further into the dynamics of the emergent behavior of spins on the hyperkagome lattice. We first reveal the existence of the director state in $\text{Gd}_3\text{Al}_5\text{O}_{12}$ (GAG), isostructural to GGG, thus showing that such emergent behavior is not unique to GGG. We further probe the low energy magnetic dynamics in GGG and GAG using AC magnetic susceptibility and inelastic neutron scattering with μeV and meV energy resolution. Finally, we discuss how the magnetic excitations can be understood in terms of a combination of single spin dynamics and collective dynamics on the ten-ion loops.

II. BACKGROUND

GGG is a well known magnetically frustrated compound with Gd^{3+} ions positioned on a three dimensional hyperkagome lattice. The Gd^{3+} ions have $S = 7/2$ and are usually regarded as spherically symmetric, although there are indications of a weak planar anisotropy stemming from crystal field effects^{6,14}. The space group of GGG is $\text{Ia}\bar{3}\text{d}$, with $a = 12.39$ Å. The Curie-Weiss temperature of GGG is $\theta_{CW} \sim -2.25$ K and neighboring spins are coupled with an antiferromagnetic exchange of $J_1 = 107$ mK¹⁵. No conventional long-range magnetic order has been found down to 25 mK¹⁶. Neutron scattering revealed the onset of short-range correlations for $T < 4$ K with the director correlations developing for $T \lesssim 1.5$ K^{6,16}. Below $T_f^{\text{GGG}} = 175$ mK, the spins freeze partially^{17–19}. The freezing is a result of the interplay between the next nearest exchange interaction, $-12 \text{ mK} \leq J_2 \leq 4$ mK, the inter-sublattice exchange interaction, $-3 \text{ mK} < J_3 < 12$ mK, and the long-range dipole interaction, \mathcal{D} ²⁰. The magnetic behavior of GGG can be modeled using a standard Heisenberg model¹³:

$$\mathcal{H} = \sum_{ij} J_{ij} \mathbf{S}_i \cdot \mathbf{S}_j + \mathcal{D} \sum_{ij} \frac{\mathbf{S}_i \cdot \mathbf{S}_j - 3(\mathbf{S}_i \cdot \hat{\mathbf{r}}_{ij})(\mathbf{S}_j \cdot \hat{\mathbf{r}}_{ij})}{r_{ij}^3}, \quad (1)$$

where $\hat{\mathbf{r}}_{ij}$ is a unit vector between atoms i and j .

In comparison to GGG, GAG has a larger near-neighbor exchange constant of $J_1 = 186$ mK¹⁹, and the magnitude of the Curie-Weiss constant is larger as well, $\theta_{CW} \sim -3.9(3)$ K. The further-neighbor exchange constants are presently unknown for GAG. The (H, T) phase diagram determined for GAG¹⁹ is similar to that of GGG^{17,21} with phase boundaries normalised to the magnitude of J_1 . A spin freezing in GAG happens below $T_f^{\text{GAG}} \sim 300$ mK. The dipolar interaction strength, \mathcal{D} , in GAG and GGG, calculated using the near-neighbor Gd distances in each compound, are similar, being slightly larger in GAG (48 mK) than in GGG (45 mK). The ratio \mathcal{D}/J_1 is thus smaller in GAG than in GGG by a factor 0.6. The parameters for GGG and GAG are summarized in Table I.

	θ_{CW}	J_1	\mathcal{D}	\mathcal{D}/J_1	T_f
GGG	-2.25 K	107 mK	45 mK	0.42	175 mK
GAG	-3.9(3) K	186 mK	48 mK	0.26	300 mK

Table I. Relevant magnetic parameters for GGG and GAG as discussed in the text.

III. EXPERIMENTAL DETAILS

We have carried out several experiments on powdered samples of GAG and GGG, previously used in Ref. 19

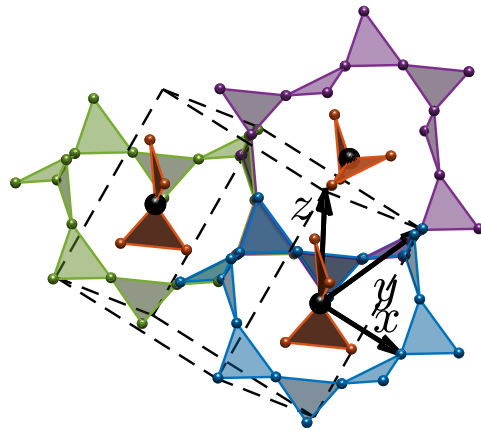


Figure 1. The environment of a Gd^{3+} atom on the hyperkagome lattice in GGG and GAG, showing the local coordinate system and the ten-ion loop surrounding each atom. The central (black) atom is representative of the director position. The interplay between three different ten-ion loops are shown. The unit cell is shown with dashed lines. Not all Gd atoms in the unit cell are shown.

and Refs. 9, 21, and 22 respectively. Both samples use isotopically enriched ^{160}Gd (99.98% for GGG, 98.4% for GAG) to reduce the neutron absorption cross-section.

We have performed a polarized neutron powder diffraction experiment on 1.6 g of GAG on the diffuse scattering spectrometer D7 at the Institut Laue Langevin (ILL)^{23,24}. The sample was cooled using a dilution refrigerator, to access the temperature regime $60 \text{ mK} < T < 5$ K. The magnetic signal was separated from the nuclear and spin incoherent signal using the 10-point method²⁵. We corrected for finite polarization using a quartz standard and for detector efficiency using a vanadium standard²⁶. These corrections were carried out using the Large Array Manipulation Program, LAMP²⁷. Leaked signals at Q -values corresponding to strong nuclear Bragg peaks from the copper sample container were removed. The data were normalized to mbarns/sr/ Gd^{3+} by refining the nuclear structure using Fullprof²⁸.

The magnetic dynamics of powdered GAG on the meV scale were measured using the cold neutron multi-chopper spectrometer LET at ISIS^{29,30} using incident energies $E_i = 1.25, 2.0, 3.96$ and 8.69 meV with an elastic energy resolution of $0.023(1), 0.042(1), 0.11(1)$ and $0.42(1)$ meV, respectively (full width at half maximum (FWHM)), determined using an incoherent scatterer. The data were reduced using Mantid³¹. We measured the magnetic dynamics at three temperatures (50 mK, 500 mK and 1 K). The slow magnetic dynamics of powdered GGG on the μeV scale were measured using the neutron backscattering instrument IN16b of the ILL^{32,33}, across a temperature range $60 \text{ mK} < T < 1$ K, using a dilution refrigerator. The neutron data were converted from acquisition channel to energy using standard treatments using LAMP²⁷. The instrumental resolution function can be described by a Gaussian with weak

Lorentzian tails, FWHM of $0.94(2) \mu\text{eV}$, determined using a vanadium standard.

In all neutron scattering experiments the samples were cooled for 24 hours prior to measurements to ensure that base temperature was reached.

AC susceptibility measurements were performed using a superconducting quantum interference device magnetometer equipped with a miniature dilution refrigerator, developed at the Institut Néel, Grenoble³⁴. Powders of GGG (17.13 mg) and GAG (5.7 mg) were cooled in zero applied magnetic field, and measured at temperatures down to 80 mK with the frequency varied between 0.057 Hz and 1110 Hz under an applied field of $\mu_0 H_{AC} = 0.055$ mT. In these low temperature measurements, the samples were mixed with Apiezon N grease to ensure thermalization. Furthermore, a single crystal of GGG was measured at frequencies down to 1 mHz with the AC field applied along the (110) direction.

IV. RESULTS AND DISCUSSION

A. Magnetic structure of GAG

Fig. 2(a) shows the magnetic scattering cross section, $S(Q)$, of powdered GAG as a function of wave vector transfer, Q , at 60 mK, measured at D7. It is worth noting that no energy analysis is performed on D7, and the observed signal is thus integrated over energy. This means that low energy magnetic excitations contribute to the observed diffraction signal. However, from the LET experiment on GAG presented in the next section we find that 97.4% of the energy integrated signal is within the elastic line, and the low energy magnetic excitations thus contribute only 2.6% to the total magnetic and nuclear scattering. At the peak near $Q = 1.1 \text{ \AA}^{-1}$ more than half of the total signal observed at D7 is magnetic. Therefore, the observed magnetic signal at D7 is at least $\sim 95\%$ elastic scattering, and the small contribution from inelastic scattering can safely be ignored.

The broad diffuse peaks around $Q = 1.1 \text{ \AA}^{-1}$, $Q = 1.8 \text{ \AA}^{-1}$ and $Q = 2.9 \text{ \AA}^{-1}$ are similar to those observed in GGG¹⁶, and indicate the presence of short-range magnetic order. In GGG, a detailed Reverse Monte Carlo (RMC) analysis further showed that the shape of the peaks at $Q = 1.1 \text{ \AA}^{-1}$ and 1.8 \AA^{-1} , is a signature of the director correlations⁶. We have carried out a similar analysis of our GAG data using the RMC program SPINVERT as explained below³⁵.

The SPINVERT analysis was performed using a magnetic supercell of $6 \times 6 \times 6$ unit cells with a spin on each of the magnetic sites. We found $n = 6$ (5184 spins) to be the smallest unit cell to yield a refinement consistent with our data. The spins were treated as classical vectors, an approximation which is justified by the large spin of Gd^{3+} and the localized nature of the spins. Each simulation was initiated with every spin pointing along a random direction. In each Monte Carlo step a ran-

dom spin was rotated slightly, and the powder averaged magnetic neutron diffraction signal from the spin configuration was calculated and scaled by a constant scale factor, $s = g^2 S(S+1) = 63$, then compared with the experimental data. The new spin orientation was kept or rejected using the Metropolis algorithm³⁶. We carried out 100 independent simulations for each temperature, with 100 steps per Gd^{3+} ion, resulting in 518400 steps for each simulation. Data presented are an average of these 100 simulations. We note that unlike direct Monte Carlo, this procedure provides no information on the relevant exchange interactions, but does yield a spin structure consistent with the neutron scattering data.

The resulting RMC fit is shown as a continuous red line through the data points in Fig. 2(a), showing excellent agreement with the data. The finite system size makes the calculation unreliable for $Q < 2\pi/(na/2) \leq 0.17 \text{ \AA}^{-1}$, indicated by the dashed black line.

We now look at the RMC spin structure to determine the local spin directions and any director correlations. Fig. 2(c) shows a three dimensional histogram of the local orientation of each Gd^{3+} spin at 60 mK, normalized by the solid angle of the bin. Similar to GGG we find a strong local xy -anisotropy. It is possible that the anisotropy originates from the dipolar interaction⁶. Fig. 2(d) shows the magnitude of the spin-spin correlations averaged over shells at distance r , $|\langle \mathbf{S}(0) \cdot \mathbf{S}(\mathbf{r}) \rangle|$. We find antiferromagnetic near-neighbor correlations which follow an approximate exponential decay, $\langle \mathbf{S}(0) \cdot \mathbf{S}(\mathbf{r}) \rangle \approx \exp(-r/\xi)$, with $\xi = 4.2(1) \text{ \AA}$. For near neighbors we find $\langle \mathbf{S}(0) \cdot \mathbf{S}(\mathbf{r}) \rangle = -0.41(1)$. This corresponds to an average angle between near-neighbor spins of 114° , significantly lower than the 120° expected for a pure Heisenberg spin state. In GGG a much smaller deviation was found, 118° .

In GGG it was found that the spin structure depends strongly on the precise values of J_1 , J_2 and J_3 , and their interplay with the dipolar interaction²⁰. The same is true for GAG, but since J_2 and J_3 presently are unknown in GAG, we cannot quantify their effect on the spin structure.

In order to look for evidence of the director state we follow Ref. 6 and define the 10-spin directors, \mathbf{L} as the staggered magnetization of a loop

$$\mathbf{L} = \sum_{n=1}^{10} (-1)^n \mathbf{S}_n. \quad (2)$$

The distribution of directors in GAG is shown in Fig. 2(e), revealing a strong local z anisotropy, as also found in GGG. The correlation between directors can be quantified as

$$g(r) = 2\langle |\hat{\mathbf{L}}(0) \cdot \hat{\mathbf{L}}(\mathbf{r})| \rangle - 1, \quad (3)$$

where $\hat{\mathbf{L}} = \mathbf{L}/L$. The director-director correlation is $g = 1$ for directors that are parallel, and $g = -1$ for directors that are orthogonal. We show $g(r)$ in Fig. 2(f). The near-neighbor director-director correlation is strong, which is

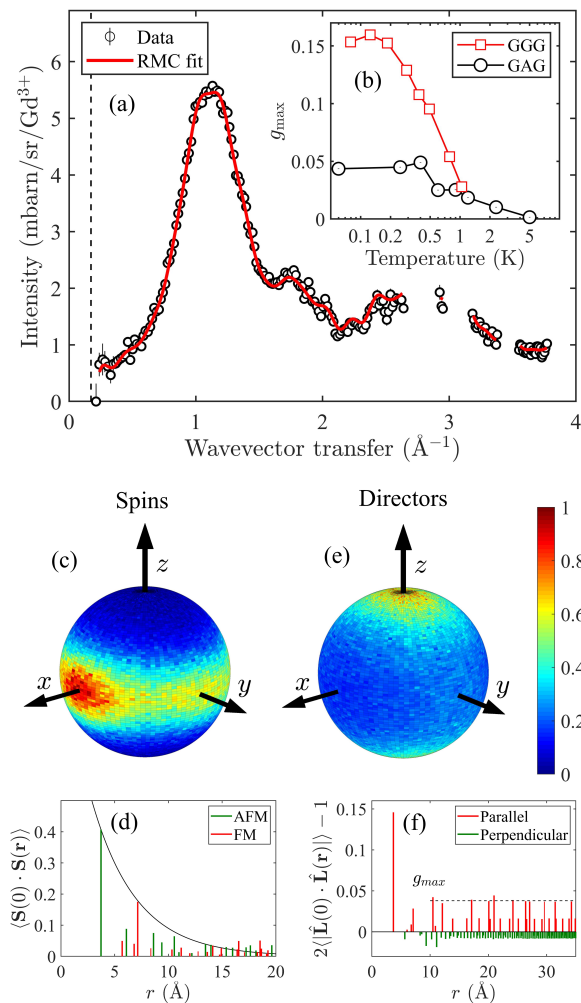


Figure 2. (a) Magnetic $S(Q)$ at $T = 60$ mK for GAG. The red line is a RMC fit using SPINVERT as described in the text. The dashed line indicates the lower limit for the RMC calculation. (b) Temperature dependence of the loop order parameter g_{\max} for GAG and GGG⁶. (c) The relative distribution of spin orientations at $T = 60$ mK in the local coordinate system shown in Fig. 1. (d) The average spin-spin correlation at $T = 60$ mK as a function of the distance between the spins, r . Green bars show antiferromagnetic correlations, $\langle \mathbf{S}(0) \cdot \mathbf{S}(\mathbf{r}) \rangle < 0$, while red bars show ferromagnetic correlations, $\langle \mathbf{S}(0) \cdot \mathbf{S}(\mathbf{r}) \rangle > 0$. The black line is the function $\exp(-r/\xi)$ with $\xi = 4.2(1)$ Å. (e) The relative distribution of director orientations at $T = 60$ mK in the local coordinate system shown in Fig. 1. (f) The correlation, $g = 2\langle \hat{\mathbf{L}}(0) \cdot \hat{\mathbf{L}}(\mathbf{r}) \rangle - 1$, between directors at $T = 60$ mK as a function of the distance between them r . The dashed line indicates the saturation level, g_{\max} , at high r .

unsurprising, as neighboring directors share several spins. Importantly, the director-director correlations then falls to a constant value, g_{\max} , that extends beyond 30 Å. As such we find that the directors in GAG remain correlated, albeit weakly, over long distances.

Fig. 2(b) shows the temperature dependence of g_{\max}

for GGG and GAG. Both compounds show an increase in g_{\max} below 1.5 K, as the director state emerges. g_{\max} increases rapidly with decreasing temperatures, and peaks at ~ 400 mK and 175 mK for GAG and GGG, respectively. Below this temperature, which coincides roughly with the onset of the spin freezing^{17–19}, g_{\max} appears to remain constant. $g_{\max}(\text{GGG}) \approx 3g_{\max}(\text{GAG})$ indicating that the director-director correlations at the lowest temperatures are stronger in GGG than in GAG.

This difference is likely caused by a combination of variations in J_2 and J_3 , as well as the variation in \mathcal{D}/J_1 , with \mathcal{D}/J_1 for GAG being smaller by a factor 0.6. It would be interesting to study other Gd³⁺ based garnets with different values of \mathcal{D}/J . For example, Gd₃Te₂Li₃O₁₂ (GTLG) has $\mathcal{D}/J = 0.36$ ¹⁸, and we therefore predict a director state to be present in GTLG with $0.05 < g_{\max}^{\text{GTLG}} < 0.15$. Ref.³⁷ also suggests multiple Gd³⁺-based garnets with varying values of \mathcal{D}/J_1 that would be interesting to study. It would also be valuable to determine J_2 and J_3 for GAG. For GGG, the most accurate determination of these parameters was based on an analysis of the longer-range correlations that set in in GGG for temperatures below 175 mK²⁰. Such correlations are not present in GAG, making a similar analysis impossible at present.

The presence of director correlations in GAG as well as in GGG indicate that any hyperkagome system with antiferromagnetic near-neighbor interactions and relatively strong dipolar interactions should display a director state.

A recent study of the isostructural compound Yb₃Ga₅O₁₂, (YbGG), also reveals a director state. However, in stark contrast to GGG and GAG, the director state in YbGG is derived from ferromagnetic near-neighbor exchange, with spins directed along the local z direction³⁸, with directors correlated over short distances. Despite these differences, the director state on hyperkagome lattices thus appears to be rather robust. To form a director state, some form of anisotropy in the spin orientation seems to be required. In GGG and GAG, this anisotropy is most likely a result of the dipolar interaction, with the potential addition of small crystal field effects, whereas the anisotropy in YbGG originates almost entirely from crystal field effects. The precise interactions which determine whether the director state is long- or short-range are unclear.

B. meV dynamics of GAG

Fig. 3 shows $S(Q, E)$, at 50 mK for GAG measured at LET using incident energies $E_i = 3.69$ and 2.0 meV. We observe three distinct features, similar to previous results on GGG⁹. We label the three features INS1, INS2 and INS3 in line with the nomenclature employed for GGG.

INS3 is a weak non-dispersive excitation observed at 0.588(5) meV, shown in Fig. 3(a). The intensity of this excitation does not follow a single ion form factor, and

is thus not a crystal field excitation. In GGG this excitation was found at $0.58(3)$ meV⁹. At lower energies, Fig. 3(b), we observe two further distinct features, labelled INS1 and INS2. Within the energy resolution and statistics afforded by the experiment INS1 is a low-lying dispersionless excitation at $E = 0.05(1)$ meV with INS2, a much broader feature that is more dispersive in nature. At low Q , INS2 appears at $E = 0.19$ meV and falls into the elastic line near $Q \sim 1 \text{ \AA}^{-1}$. All three excitations have slightly higher energies in GAG than in GGG, consistent with the stronger exchange interactions in GAG.

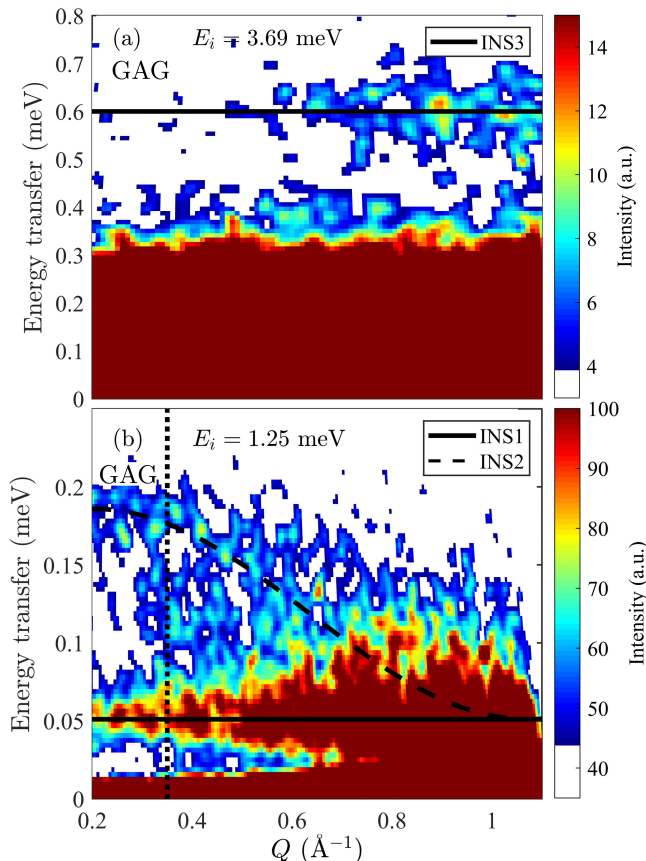


Figure 3. $S(Q, E)$ of GAG at 50 mK measured at LET with incident neutron energy (a) $E_i = 3.69$ and (b) 1.25 meV. The dashed line on (b) indicates the central position of the cuts used to quantify the temperature variations of these excitations in Figs. 4 and 5. The lines are guides to the eye, and the color scale is chosen to emphasize INS1, INS2 and INS3.

The dotted vertical line in Fig. 3(b) shows the direction of cuts through the data for a range of temperatures $T = 50$ mK, 500 mK and 1 K. The cuts are presented in Fig. 4(b). At 50 mK the three excitations are well defined and can be modeled as gapped modes. Upon increasing the temperature, the signal broadens. The gap to INS1 remains visible, but INS2 appears to become overdamped and thus transforms into almost featureless quasi-elastic scattering. INS3, in contrast, remains well defined at least up to 1 K.

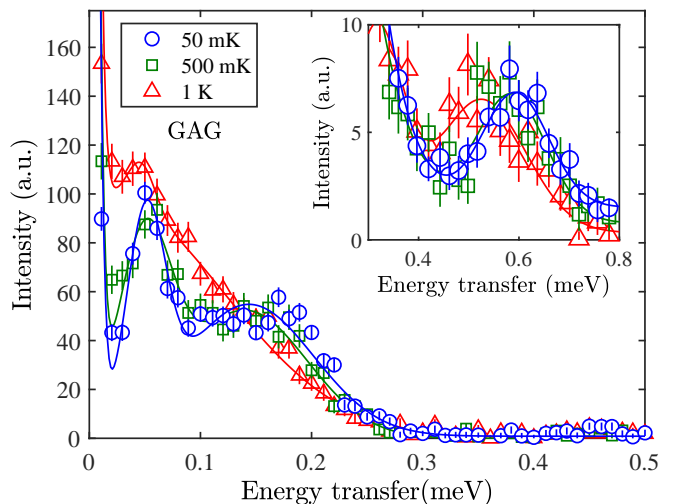


Figure 4. Temperature and energy dependence of INS1 and INS2 for GAG, measured at LET. A 0.2 \AA^{-1} wide cut of the data around $Q = 0.35 \text{ \AA}^{-1}$ at 0.05, 0.5 and 1 K, shows the existence of two low-lying excitations. The inset shows the Q integrated intensity of INS3. Continuous lines are fits to the data.

The temperature dependence of the position of INS3 is similar to GGG, see Fig. 5(a). Fig. 5(b) shows the resolution-corrected half width at half max (Γ) of the INS3 peak in GAG and GGG and the excitation lifetime, $\tau = \hbar/\Gamma$. At elevated temperatures the excitation life time is nearly identical in the two compounds⁹. The solid line is a guide to the eye.

A magnetic field study by d'Ambrumenil et al. of the magnetic excitations in GGG have previously provided theoretical insight into the excitations of GGG¹³. d'Ambrumenil et al. accurately reproduced the full dispersion of GGG in an applied magnetic field using linear spin-wave theory on the ten-ion loops, including near-neighbor interactions and the dipolar interaction. This study was carried out in a magnetic field large enough to create a ferromagnetic ground state, very different from the zero-field ground state. Still, the dispersion is similar in both applied and zero field, indicating that the underlying excitations are similar. Comparing our results with those of Ref.¹³ suggests that INS1 originates from bands that are near dispersion-less across the entire Brillouin Zone. INS2, on the other hand, consists of multiple dispersive excitations that cross and overlap in reciprocal space.

No equivalent of INS3 is found by linear spin wave theory in the ordered state, and it may therefore have an entirely different origin. The mode is relatively sharp in energy, and has a strikingly similar position and width in the two compounds. The lack of scaling with J_1 suggests that near-neighbor interactions is not the main driver of this excitation. In GGG, the INS3 mode was modeled as a singlet-triplet excitation, based on the Q -dependence of the intensity⁹. Due to the weak signal we could not

extract the Q -dependence of the intensity in GAG, and thus cannot verify if this model fits the present data.

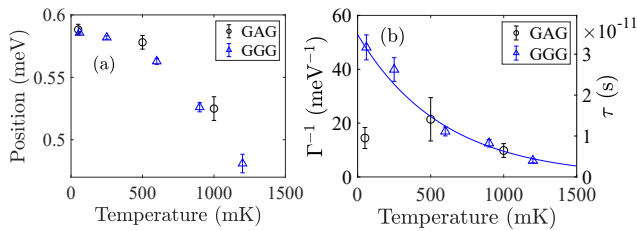


Figure 5. (a) Temperature dependence of the position of the INS3 excitation for GAG and a GGG. (b) Temperature dependence of the fluctuation rate expressed as the inverse of the HWHM of the peak. The solid line is a guide to the eye.

C. μeV dynamics of GGG

An overview of the backscattering data, $S(Q, E)$, for GGG is shown in Fig. 6 for $60 \text{ mK} < T < 1 \text{ K}$. At all temperatures a strong elastic signal is present for all accessible wavevector transfers. At the lowest temperature probed, 60 mK, the signal appears almost entirely elastic. A broad quasielastic broadening is observed around 450 mK with a peak in intensity near wavevector transfer $Q = 1.1 \text{ \AA}^{-1}$. At 1 K the quasi-elastic signal has broadened further and reaches the edge of the experimental energy window.

The energy dependence of the total scattering signal is well described, for all scattering vectors and temperatures, by a convolution of the resolution function with a temperature independent elastic term, represented by a delta function, and a temperature dependent quasi-elastic Lorentzian term

$$I = R \otimes \left(A_{\text{el}} \delta(E) + \frac{A_{\text{qel}}}{\pi} \frac{\Gamma}{\Gamma^2 + E^2} \right) + C_1 + C_2 E, \quad (4)$$

where R is the resolution function, A_{el} is the integrated intensity of the elastic signal, and A_{qel} is the intensity of the quasielastic signal, 2Γ is the FWHM of the quasielastic signal. A linear sloping background is included, described by the parameters C_1 and C_2 . We have accounted for detailed balancing in the fitting³⁹, although the effect is minimal. Fig. 7 shows an example of the data (black circles) and fit (red solid line) at 450 mK and $Q = 1.1 \text{ \AA}^{-1}$. We see a significant quasielastic broadening, compared with the instrumental resolution (dashed green line).

The inset of Fig. 7 shows the temperature dependence of the wavevector integrated intensity, which follows the trend seen in Fig. 6. The temperature dependence of the Lorentzian signal indicates its magnetic origin.

The most important fitted parameters are shown in Fig. 8, and the background parameters are discussed in the appendix. The Q - and temperature dependence of

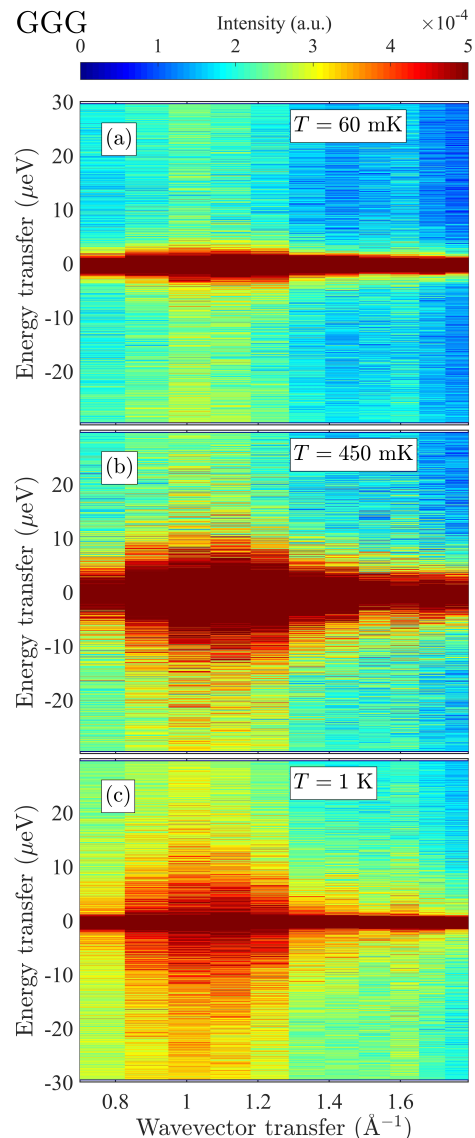


Figure 6. $S(Q, E)$ of GGG measured at IN16b at temperatures $T = 60 \text{ mK}$, 450 mK and 1 K .

the integrated intensity of the Lorentzian signal, A_{qel} , is shown in Fig. 8(a). The integrated intensity, with broad peaks at $Q = 1.1$ and 1.8 \AA^{-1} , follows the Q dependence of the elastic magnetic structure factor previously determined for GGG²², and shown for GAG in Fig. 2(a). The temperature dependence of the integrated intensity of the quasi-elastic component, A_{qel} at $Q = 1.1 \text{ \AA}^{-1}$ is shown in Fig. 8(c). It remains roughly constant for $T < 0.2 \text{ K}$ and decreases rapidly with increasing temperature, consistent with the decrease of magnetic correlations with increasing temperature.

The temperature and Q dependence of the FWHM of the quasi-elastic signal, 2Γ , is shown in Fig. 8(b). It is interesting to note that Γ is independent of Q in the accessible range ($0.7 \text{ \AA}^{-1} < Q < 1.8 \text{ \AA}^{-1}$), but increases rapidly with increasing temperature. The lack of Q -dependence

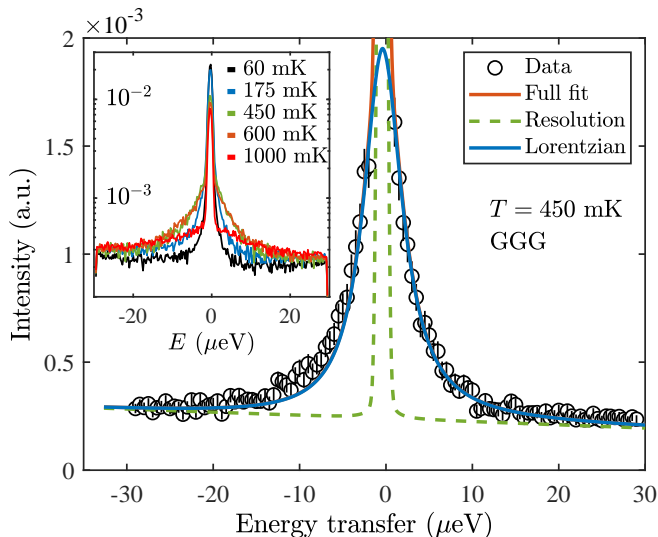


Figure 7. Example of IN16b data on GGG at 450 mK for $Q = 1.1 \text{ \AA}^{-1}$. The solid red line is a fit as described in the text. The solid blue line is the Lorentzian contribution. The dashed green line shows the resolution function on top of the background. The inset shows the temperature dependence of the data on a log scale.

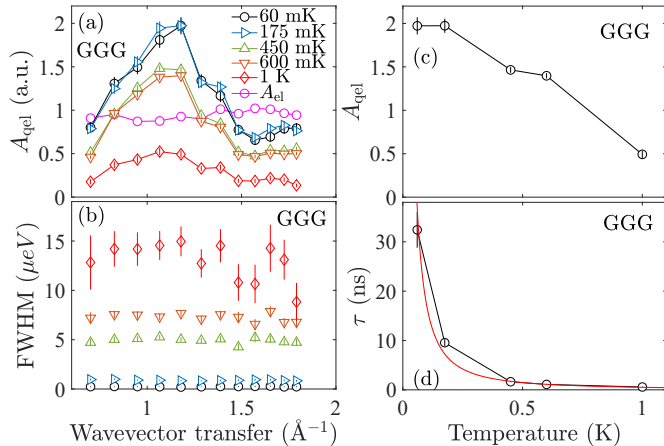


Figure 8. (a) Q dependence of the area of the Lorentzian signal, A_{qel} measured on GGG at IN16b, showing peaks at $Q=1.1$ and 1.8 \AA^{-1} , indicating that this signal is magnetic. (b) The resolution-corrected FWHM of the Lorentzian signal (2Γ), displaying no significant Q dependence. (c) Temperature dependence of A_{qel} . (d) Temperature dependence of the relaxation rate, $\tau = \hbar/\Gamma$, along with a fit to $\tau = AT^B$, with $B = -1.5(3)$.

indicates that the spin fluctuations are uncorrelated on this energy scale, a surprising result given the existence of both director and static spin-spin correlations in GGG.

A single Lorentzian lineshape indicates that the temporal spin-spin correlations decay as

$$\langle \mathbf{S}(0) \cdot \mathbf{S}(t) \rangle \sim e^{-t/\tau}, \quad (5)$$

where the decay rate, τ is related to the FWHM by

$2\Gamma = 2\hbar/\tau^{40}$. The temperature dependence of τ at $Q = 1.1 \text{ \AA}^{-1}$ is shown in Fig. 8(d) and follows $\tau = AT^B$, with $B = -1.5(3)$. Our results are consistent with earlier Mössbauer measurements on GGG¹² as well as muon spin rotation measurements^{10,11}, who all found spin fluctuations in GGG on a similar time scale as presented here. In the Mössbauer measurements, the temperature dependence was quadratic¹² and the fluctuations were shown to be confined to a plane, consistent with the spin anisotropy mentioned earlier⁶.

Significant theoretical work has been performed on the spin fluctuation rate for a system of classical spins on frustrated lattices. Conlon and Chalker predicted, for Heisenberg spins on a pyrochlore lattice in a cooperative paramagnetic regime, a linear temperature dependence of the spin fluctuation rate (τ^{-1}) with spin correlations that relax at a rate independent of the wavevector transfer⁴¹. The hyperkagome lattice can be viewed as a depleted pyrochlore lattice, where each tetrahedron is missing a site. As such, we can expect the magnetic behavior on these two systems to be similar. In GGG, for $T < 1$ K, the spin correlations are indeed independent of Q , although τ follows a power law rather than being linear.

More recently, the diffusive dynamics on frustrated kagome lattices have been investigated. Taillefumier predicts a distribution of timescales in the cooperative paramagnetic regime representing loops diffusing in an entropically dominated free energy landscape. The signature of such diffusion can be observed for $Q < 2\pi/d$ where $d = a$ is the loop spatial scale. In this Q region, τ^{-1} increases linearly with Q ⁴². Unfortunately, we do not access a wavevector transfer below 0.7 \AA^{-1} , and thus do not directly observe this. However, in line with Taillefumier, at larger wavevector transfers the fluctuation rate is proportional to temperature and independent of Q ⁴². We therefore suggest that we are probing the diffusive dynamics of the multipolar director state in GGG. Data at lower Q is required to confirm or reject this hypothesis. Such experiments will be challenging due to the vanishing intensity at low Q as seen in diffraction experiments.

Further progress on understanding the director dynamics on the μeV and meV energy scale will also require inelastic neutron scattering experiments on single crystal samples. Such experiments are only feasible on isotope enriched single crystals to minimize the absorption of cold neutrons required to achieve the relevant energy resolutions. The cost of such crystals is prohibitively high.

Finally, we note that some magnetic scattering is seen in the apparent background signal, as it depends on temperature (see the appendix for details). This indicates that part of the background originates from motions on a larger energy scale than the accessible energy window of IN16b ($\sim \pm 30 \text{ \mu eV}$), as also found in similar backscattering measurements on $\text{Tb}_2\text{Sn}_2\text{O}_7$ ⁴⁰. It is likely that this contribution originates from the tails of the lowest excitation, INS1, observed at $0.05(1) \text{ meV}$ at the lowest temperature.

D. AC susceptibility

AC susceptibility is a very sensitive probe of low frequency magnetic dynamics⁴³. In our AC susceptibility measurements we measure the real (χ') and imaginary susceptibility (χ''), for both GGG and GAG as a function of temperature.

Fig. 9(a) shows χ' for a single crystal of GGG with the AC field applied along the [110] direction. An anomaly around $T_f \sim 175$ mK is seen, with a slight frequency-dependence. Fig. 9(b) shows χ'' for the same single crystal, with (c) zooming in on selected frequencies. The temperature dependence of χ'' varies from a single peak for frequencies below ~ 5 Hz to a double peak structure emerging for frequencies > 5 Hz. We fitted the peaks using Gaussian line shapes to extract the position of the peaks.

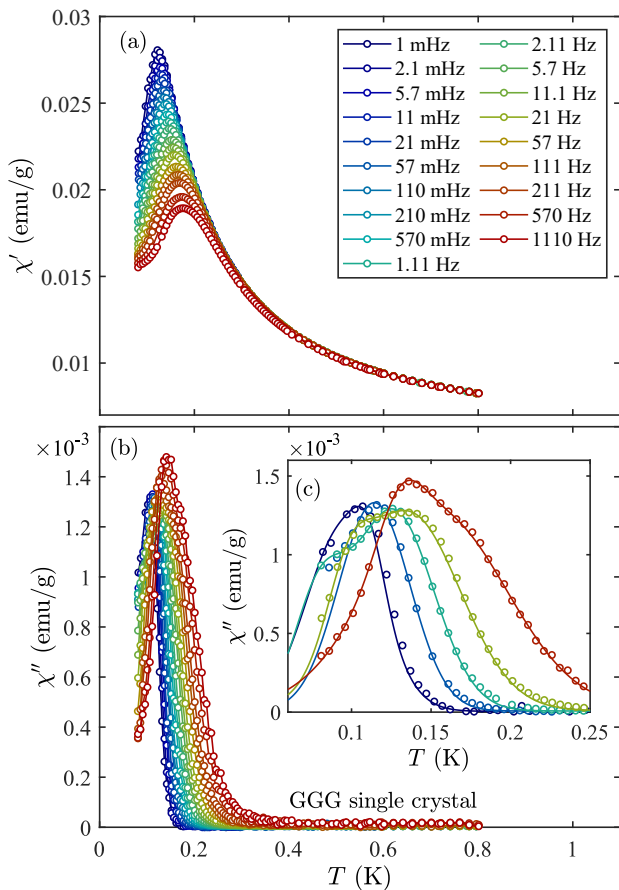


Figure 9. Temperature and frequency dependence of (a) the real (χ') and (b) imaginary (χ'') AC susceptibility on a single crystal of GGG measured along the (110) direction. The frequencies, $1 \text{ mHz} < f < 1110 \text{ Hz}$, are indicated by color. (c) Detailed view of χ'' for selected frequencies. Continuous lines are fits to Gaussians as described in the text.

The frequency dependence of the peak position of these curves follows an Arrhenius temperature dependence, see

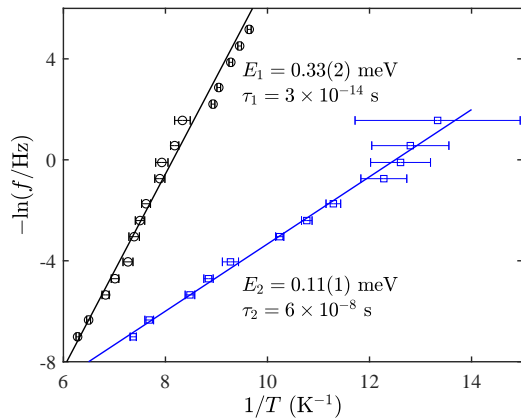


Figure 10. Arrhenius plot for the two peaks in χ'' for the single crystal of GGG. The straight lines are fits to the Arrhenius law as described in the text.

Fig. 10.

$$\tau_i = \tau_{0,i} e^{E_{a,i}/k_B T}, \quad (6)$$

where $i = 1, 2$, E_i is an activation energy and $\tau_{0,i} = 2\pi/f$ the relaxation lifetime of spin vector reversal. The excellent fit to the Arrhenius law indicates that the motion of the spins on this energy scale is governed by thermal activation across an energy barrier. Two distinct peaks indicate two distinct relaxation processes.

The fits to the data using the Arrhenius law for each of the two peaks provide activation energies of $E_{a,1} = 0.33(2) \text{ meV}$ ($3.8(3) \text{ K}$) and $E_{a,2} = 0.11(1) \text{ meV}$ ($1.3(2) \text{ K}$) and relaxation lifetimes of $\tau_{0,1} = 3 \times 10^{-14} \text{ s}$ and $\tau_{0,2} = 6 \times 10^{-8} \text{ s}$. It should be noted that the uncertainty on τ is about an order of magnitude. The energy barriers are the same order of magnitude as the excitation energies probed with neutron scattering.

The temperature dependence of χ' for powdered GGG is given in Fig. 11(a) for $f = 57, 111$ and 211 Hz . Two anomalies are seen, near 350 mK and 100 mK , as also found previously⁴⁴. The signal is much broader than for the single crystal, and the two anomalies are at different temperatures than the anomaly in χ' for the single crystal of GGG.

Fig. 9(b) shows the temperature dependence of χ' for powdered GAG for a larger range of frequencies. Here, a single, broad peak is seen around 350 mK . The broadness of the peak indicates a broad distribution of time scales in the system.

The temperature dependence of χ'' is shown in Fig. 9(c) for GGG and Fig. 9(d) for GAG. In both cases a broad anomaly is seen around 250 mK . The peaks in the powdered data are substantially broader than the single crystal data on GGG, which indicates the existence of a broader distribution of relaxation times in the system. In both compounds the peak temperature of χ'' depends very weakly on frequency. However, fitting to an Arrhenius law, gives unphysical characteristic times, suggesting that the freezing mechanism is more complex,

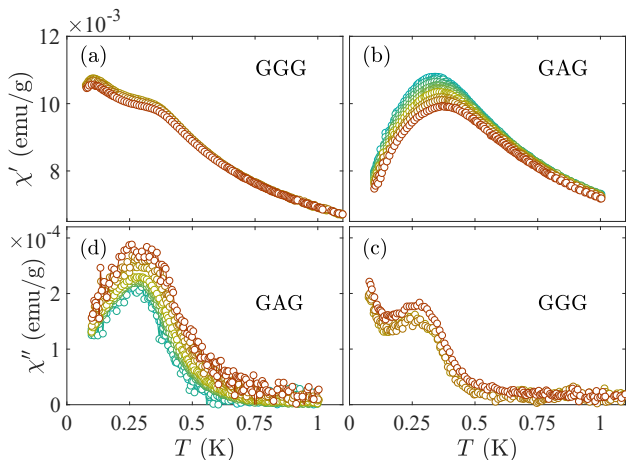


Figure 11. Temperature and frequency dependence of the real (χ') and imaginary (χ'') AC susceptibility on powders of GGG. The frequencies, $0.57 < f < 211$ Hz, are indicated by the same colors as in Fig. 9. (a) χ' for powdered GGG. (b) χ' for powdered GAG. (c) χ'' for powdered GGG. (d) χ'' for powdered GAG.

and cannot be explained with a single energy barrier. Modifications to the Arrhenius law, such as the Vogel-Fulcher law⁴⁵, can be made to fit the data with sensible parameters, but the correlations between fitted parameters become so large that interpretation of their values is meaningless. Instead, the frequency dependence of the χ' peak can be analyzed through the Mydosh parameter K , frequently used to describe spin glasses,

$$K = \frac{\Delta T_f}{T_f \Delta \log(f)}, \quad (7)$$

where T_f is the temperature of the χ' maximum. For the GGG powder, we have insufficient data to determine K . For GAG, we obtain $K_{\text{GAG}} = 0.03 - 0.04$, which falls in the range of insulating spin-glasses, if a bit smaller⁴⁶. Nevertheless, the broad shape of the χ' features in GAG and of the ZFC-FC magnetization¹⁹ seems to preclude a conventional spin-glass transition. In particular, we could not accurately determine the freezing temperature T_g which would have allowed us to perform dynamical scaling and estimate possible critical exponents. Further measurements, in a larger frequency range are thus needed to conclude on the nature of the freezing in GAG. The broad feature is reminiscent of the heterogeneous freezing scenario proposed for Heisenberg kagomé antiferromagnets⁴⁷, and thus suggests that multiple time and lengths scales are involved in this relaxation mechanism.

Our AC susceptibility measurements on GGG and GAG confirm the spin freezing upon cooling below ~ 175 mK and ~ 300 mK respectively, with a frequency dependent χ' and χ'' . Most interestingly, the temperature dependence of χ'' for the single crystal of GGG displays an unusual double peaked structure. The frequency depen-

dence of each peak follows an Arrhenius law, thus indicating the presence of two distinct thermally activated processes. Single spin magnetization precession is typically on the ps timescale, e.g. Ref. 48, indicating that the first process in GGG, with $\tau_0 = 3 \times 10^{-14}$ s, is related to single spin reversal. The second process ($\tau_0 = 6 \times 10^{-8}$ s) is too slow to involve single spins, and is thus probing the dynamics of larger structures, which we can reasonably assume to be the ten-ion loops. These results differ from those by Ghosh et al.⁸ who probed the ten-ion looped structure using magnetic hole burning and found temperature independent clusters behaving as quantum objects. In our case the signatures remain thermally driven.

In contrast to the single crystal measurements on GGG, the temperature dependence of the powdered GAG AC susceptibility displays a very broad single peaked structure, from which we could not extract a characteristic energy scale. Most probably, a wide distribution of correlation lengths is involved in this dynamical process, which is consistent with the smaller strength of the ten-ion loops correlations in GAG compared with GGG. The larger deviation from the 120° spin structure in GAG than in GGG obtained in the diffraction measurements may also explain the differences between the observed slow dynamics.

V. SUMMARY AND CONCLUSION

In summary, we have presented an extensive comparative study of GGG and GAG using neutron diffraction, neutron backscattering and time-of-flight spectroscopy and AC susceptibility. We confirm the existence of long range director correlations in GAG, and propose that it will be present in all garnets with antiferromagnetic near-neighbor exchange and relatively strong dipolar interaction or local xy -anisotropy. The reduced D/J_1 value in GAG as well as possible changes in J_2 and J_3 result in weaker director correlations.

On the meV scale, GGG and GAG show similar dynamics with three distinct excitations, INS1-3. In particular, the temperature dependence of the excitation energy and lifetime of the INS3 excitation at 0.58 meV is nearly identical in the two compounds, indicating that it is not driven by near neighbor exchange interactions. The other two excitations are reminiscent of spin waves found in the polarized state of GGG.

On the μeV scale, the spins in GGG fluctuate with a rate that decreases as $T^{1.5}$. The fluctuations are independent of wavevector transfer in the probed range, consistent with the presence of spin diffusion. The slowest dynamics probed by AC susceptibility with low frequencies reveal two distinct fluctuation processes in GGG. One of these is associated with single spin fluctuations, while the other is associated to larger structures, most likely the directors. AC susceptibility on powders of GGG and GAG furthermore give insight into the nature of the freezing of the spins that occurs at low temperature.

We have suggested several directions for further experimental and theoretical work: On the experimental side it would be interesting to ascertain the presence of director correlations in other Gd-based hyperkagome systems, such as $\text{Gd}_3\text{Te}_2\text{Li}_3\text{O}_{12}$. In addition, experimental work to determine the further-neighbor exchange constants in GAG would be valuable.

Based on our AC susceptibility data we expect the μeV dynamics of GAG to be different from GGG. This prediction can be straightforwardly tested experimentally on powders of GAG. To determine if the Q -independence of the quasi-elastic broadening is caused by spin diffusion or uncorrelated fluctuations, we propose two experiments: First, similar backscattering experiments as presented here, but reaching lower Q -values, would reach the regime where the width of the signal decreases linearly with decreasing Q in a spin diffusion model. Such an experiment will be difficult due to the small magnetic signal at the required low Q . Second, measurements on an isotope enriched single crystal would reveal any Q -dependence on the signal which is currently lost in powder averaging. Unfortunately, ^{160}Gd is extremely expensive.

With an isotope enriched single crystal the meV dynamics could also be studied further. We expect INS2 to consist of multiple broad bands of excitations that are similar in nature to the excitations found in the field-polarized state.

Finally, it is also clear that more theoretical work is required. The origin of the INS3 excitation remains unclear, as does the exact nature of the excitations associated with the director correlations. Conventional spin wave theory is not applicable to these systems, but another avenue to approach this problem could be numerical Langevin simulations.

ACKNOWLEDGMENTS

This work was supported by the Danish Council for Independent Research through DANSCATT. This work is based on neutron scattering experiments performed at Institut Laue-Langevin, France, and at ISIS, UK.

Experiments at the ISIS Neutron and MuonSource were supported by beam-time allocations from the Science and Technology Facilities Council.

The work was supported by MAX4ESSFUN as part of the Interreg project ESS&MAX IV Cross Border Science and Society, Ref. no. KU-001. HJ acknowledges funding from the EU Horizon 2020 programme under the Marie Skłodowska-Curie grant agreement No701647.

We thank Rasmus Tang and Emil Martiny for useful discussions.

- ¹ T. Fennell, P. P. Deen, A. R. Wildes, K. Schmalzl, D. Prabhakaran, A. T. Boothroyd, R. J. Aldus, D. F. McMorrow, and S. T. Bramwell, "Magnetic Coulomb phase in the spin ice $\text{Ho}_2\text{Ti}_2\text{O}_7$." *Science* **326**, 415 (2009).
- ² D. J. P. Morris, D. A. Tennant, S. A. Grigera, B. Klemke, C. Castelnovo, R. Moessner, C. Czternasty, M. Meissner, K. C. Rule, J. Hoffmann, K. Kiefer, S. Gerischer, D. Slobinsky, and R. S. Perry, "Dirac Strings and Magnetic Monopoles in the Spin Ice $\text{Dy}_2\text{Ti}_2\text{O}_7$," *Science* **326**, 411 (2009).
- ³ C. Castelnovo, R. Moessner, and S. L. Sondhi, "Magnetic monopoles in spin ice," *Nature* **451**, 42 (2007).
- ⁴ S. R. Giblin, S. T. Bramwell, P. C. W. Holdsworth, D. Prabhakaran, and I. Terry, "Creation and measurement of long-lived magnetic monopole currents in spin ice," *Nature Physics* **7**, 252 (2011).
- ⁵ R. Dusad, F. K. K. Kirschner, J. C. Hoke, B. R. Roberts, A. Eyal, F. Flicker, G. M. Luke, S. J. Blundell, and J. C. S. Davis, "Magnetic monopole noise," *Nature* **571**, 234 (2019).
- ⁶ J. A. M. Paddison, H. Jacobsen, O. A. Petrenko, M. T. Fernandez-Diaz, P. P. Deen, and A. L. Goodwin, "Hidden order in spin-liquid $\text{Gd}_3\text{Ga}_5\text{O}_{12}$," *Science* **350**, 179 (2015).
- ⁷ S. Lee, C. Broholm, W. Ratcliff, G. Gasparovic, Q. Huang, T. H. Kim, and S. Cheong, "Emergent excitations in a geometrically frustrated magnet." *Nature* **418**, 856 (2002).
- ⁸ S. Ghosh, T. F. Rosenbaum, and G. Aeppli, "Macroscopic signature of protected spins in a dense frustrated magnet," *Phys. Rev. Lett.* **101**, 157205 (2008).
- ⁹ P. P. Deen, O. A. Petrenko, G. Balakrishnan, B. D. Rainford, C. Ritter, L. Capogna, H. Mutka, and T. Fennell, "Spin dynamics in the hyperkagome compound $\text{Gd}_3\text{Ga}_5\text{O}_{12}$," *Phys. Rev. B* **82**, 174408 (2010).
- ¹⁰ S. R. Dunsiger, J. S. Gardner, J. A. Chakhalian, A. L. Cornelius, M. Jaime, R. F. Kiefl, R. Movshovich, W. A. MacFarlane, R. I. Miller, J. E. Sonier, and B. D. Gaulin, "Low temperature spin dynamics of the geometrically frustrated antiferromagnetic garnet $\text{Gd}_3\text{Ga}_5\text{O}_{12}$," *Phys. Rev. Lett.* **85**, 3504 (2000).
- ¹¹ I. M. Marshall, S. J. Blundell, F. L. Pratt, A. Husmann, C. A. Steer, A. I. Coldea, W. Hayes, and R. C. C. Ward, "A muon-spin relaxation (μSR) study of the geometrically frustrated magnets $\text{Gd}_3\text{Ga}_5\text{O}_{12}$ and ZnCr_2O_4 ," *J. Phys. Condens. Matter* **14**, L157 (2002).
- ¹² P. Bonville, J. A. Hodges, J. P. Sanchez, and P. Vulliet, "Planar spin fluctuations with a quadratic thermal dependence rate in spin liquid $\text{Gd}_3\text{Ga}_5\text{O}_{12}$," *Phys. Rev. Lett.* **92**, 167202 (2004).
- ¹³ N. d'Ambrumenil, O. A. Petrenko, H. Mutka, and P. P. Deen, "Dispersionless Spin Waves and Underlying Field-Induced Magnetic Order in Gadolinium Gallium Garnet," *Phys. Rev. Lett.* **114**, 227203 (2015).
- ¹⁴ E. Lefrançois, L. Mangin-Thro, E. Lhotel, J. Robert, S. Petit, V. Cathelin, H. E. Fischer, C. V. Colin, F. Damay, J. Ollivier, P. Lejay, L. C. Chapon, V. Simonet, and R. Ballou, "Spin decoupling under a staggered field in the $\text{Gd}_2\text{Ir}_2\text{O}_7$ pyrochlore," *Phys. Rev. B* **99**, 060401(R) (2019).
- ¹⁵ W. I. Kinney and W. P. Wolf, "Magnetic interactions and short-range order in gadolinium gallium garnet," *Journal of Applied Physics* **50**, 2115 (1979).
- ¹⁶ O. A. Petrenko, C. Ritter, M. Yethiraj, and D. McK Paul, "Investigation of the Low-Temperature Spin-Liquid Behavior of the Frustrated Magnet Gadolinium Gallium Garnet," *Phys. Rev. Lett.* **80**, 4570 (1998).
- ¹⁷ P. Schiffer, A. P. Ramirez, D. A. Huse, and A. J. Valentino, "Investigation of the field induced antiferromagnetic phase transition in the frustrated magnet: Gadolinium gallium garnet," *Phys. Rev. Lett.* **73**, 2500 (1994).
- ¹⁸ J. A. Quilliam, S. Meng, H. A. Craig, L. R. Corruccini, G. Balakrishnan, O. A. Petrenko, A. Gomez, S. W. Kycia, M. J. P. Gingras, and J. B. Kycia, "Juxtaposition of spin freezing and long range order in a series of geometrically frustrated antiferromagnetic gadolinium garnets," *Phys. Rev. B* **87**, 174421 (2013).
- ¹⁹ O. Florea, E. Lhotel, H. Jacobsen, C. S. Knee, and P. P. Deen, "Absence of magnetic ordering and field-induced phase diagram in the gadolinium aluminum garnet," *Phys. Rev. B* **96**, 220413(R) (2017).
- ²⁰ T. Yavorskii, M. Enjalran, and M. J. P. Gingras, "Spin hamiltonian, competing small energy scales, and incommensurate long-range order in the highly frustrated $\text{Gd}_3\text{Ga}_5\text{O}_{12}$ garnet antiferromagnet," *Phys. Rev. Lett.* **97**, 267203 (2006).
- ²¹ P. P. Deen, O. Florea, E. Lhotel, and H. Jacobsen, "Updating the phase diagram of the archetypal frustrated magnet $\text{Gd}_3\text{Ga}_5\text{O}_{12}$," *Phys. Rev. B* **91**, 014419 (2015).
- ²² O. A. Petrenko, C. Ritter, M. Yethiraj, and D. McK Paul, "Spin-liquid behavior of the gadolinium gallium garnet," *Physica B* **241-243**, 727 (1997).
- ²³ P. P. Deen, O. Florea, H. Paul, H. Jacobsen, A. Khaplanov, C. Knee, E. Lhotel, and A. Wildes, "Magnetic frustration in 3d hyperkagome compounds," Institut Laue-Langevin (ILL), doi:10.5291/ILL-DATA.5-32-805 (2015).
- ²⁴ P. P. Deen, O. Florea, P. Henry, H. Jacobsen, C. Knee, E. Lhotel, and A. Wildes, "Emergent excitations and long range order in $\text{Gd}_3\text{Al}_5\text{O}_{12}$," Institut Laue-Langevin (ILL), doi:10.5291/ILL-DATA.5-32-795 (2014).
- ²⁵ G. Ehlers, J. R. Stewart, A. R. Wildes, P. P. Deen, and K. H. Andersen, "Generalization of the classical xyz-polarization analysis technique to out-of-plane and inelastic scattering," *Review of Scientific Instruments* **84**, 093901 (2013).
- ²⁶ J. R. Stewart, P. P. Deen, K. H. Andersen, H. Schober, J. Barthélémy, J. M. Hillier, A. P. Murani, T. Hayes, and B. Lindenau, "Disordered materials studied using neutron polarization analysis on the multi-detector spectrometer, D7," *J. Appl. Crystallogr.* **42**, 69 (2009).
- ²⁷ D. Richard, M. Ferrand, and G. J. Kearley, "Analysis and visualisation of neutron-scattering data," *Journal of Neutron Research* **4**, 33 (1996).
- ²⁸ J. Rodríguez-Carvajal, "Recent advances in magnetic structure determination by neutron powder diffraction," *Physica B: Condensed Matter* **192**, 55 (1993).
- ²⁹ R. I. Bewley, J. W. Taylor, and S. M. Bennington, "LET, a cold neutron multi-disk chopper spectrometer at ISIS," *Nucl. Instrum. Methods Phys. Res. A* **637**, 128 (2011).
- ³⁰ P. P. Deen, K. Lefmann, J. Guyon-Le-Bouffy, C. Knee, P. Henry, O. Petrenko, N. d'Ambrumenil, H. Jacobsen, and R. Bewley, "Dispersionless spin waves and field-induced magnetic order in $\text{Gd}_3\text{Al}_5\text{O}_{12}$," STFC ISIS Neutron and Muon Source, <https://doi.org/10.5286/ISIS.E.RB1520308> (2015).

- ³¹ O. Arnold, J. C. Bilheux, J. M. Borreguero, A. Buts, S. I. Campbell, L. Chapon, M. Doucet, N. Draper, R. Ferraz Leal, M. A. Gigg, V. E. Lynch, A. Markvardsen, D. J. Mikkelson, R. L. Mikkelson, R. Miller, K. Palmen, P. Parker, G. Passos, T. G. Perring, P. F. Peterson, S. Ren, M. A. Reuter, A. T. Savici, J. W. Taylor, R. J. Taylor, R. Tolchenov, W. Zhou, and J. Zikovsky, “Mantid - Data analysis and visualization package for neutron scattering and μ SR experiments,” *Nucl. Instrum. Methods Phys. Res. A* **764**, 156 (2014).
- ³² P. P. Deen, B. Frick, H. Jacobsen, and T. Seydel, “Exploring microeV dynamics in Gadolinium Gallium Garnet,” Institut Laue-Langevin (ILL), doi:10.5291/ILL-DATA.4-03-1704 (2014).
- ³³ B. Frick, E. Mamontov, L. V. Eijck, and T. Seydel, “Recent Backscattering Instrument Developments at the ILL and SNS,” *Zeitschrift für Physikalische Chemie* **224**, 33 (2010).
- ³⁴ C. Paulsen, “Introduction to physical techniques in molecular magnetism: Structural and macroscopic techniques,” (University of Zaragoza, Zaragoza, 2001).
- ³⁵ J. A. M. Paddison, J. Ross Stewart, and A. L. Goodwin, “Spinvert: a Program for Refinement of Paramagnetic Diffuse Scattering Data,” *J. Phys. Condens. Matter* **25**, 454220 (2013).
- ³⁶ N. Metropolis and S. Ulam, “The Monte Carlo Method,” *Journal of the American Statistical Association* **44**, 335 (1949).
- ³⁷ P. Mukherjee, A. C. S. Hamilton, H. F. J. Glass, and S. E. Dutton, “Sensitivity of magnetic properties to chemical pressure in lanthanide garnets $\text{Ln}_3\text{A}_2\text{X}_3\text{O}_{12}$, $\text{Ln} = \text{Gd}, \text{Tb}, \text{Dy}, \text{Ho}$, $\text{A} = \text{Ga}, \text{Sc}, \text{In}, \text{Te}$, $\text{X} = \text{Ga}, \text{Al}, \text{Li}$,” *J. Phys. Condens. Matter* **29**, 405908 (2017).
- ³⁸ L. Ø. Sandberg, R. Edberg, I. M. B. Bakke, K. S. Pedersen, M. C. Hatnean, G. Balaskrishnan, L. Mangin-Thro, A. Wildes, B. Fåk, G. Ehlers, G. Sala, P. Henelius, K. Lefmann, and P. P. Deen, “Emergent magnetic behavior in the frustrated $\text{Yb}_3\text{Ga}_5\text{O}_{12}$ garnet,” (2020), arXiv:2005.10605.
- ³⁹ A. Boothroyd, *Principles of Neutron Scattering from Condensed Matter* (Oxford University Press, Oxford, 2020).
- ⁴⁰ I. Mirebeau, H. Mutka, P. Bonville, A. Apetrei, and A. Forget, “Investigation of magnetic fluctuations in $\text{Tb}_2\text{Sn}_2\text{O}_7$,” *Phys. Rev. B* **78**, 174416 (2008).
- ⁴¹ P. H. Conlon and J. T. Chalker, “Spin Dynamics in Pyrochlore Heisenberg Antiferromagnets,” *Phys. Rev. Lett.* **102**, 237206 (2009).
- ⁴² M. Taillefumier, J. Robert, C. L. Henley, R. Moessner, and B. Canals, “Semiclassical spin dynamics of the antiferromagnetic Heisenberg model on the kagome lattice,” *Phys. Rev. B* **90**, 064419 (2014).
- ⁴³ C. V. Topping and S. J. Blundell, “A.C. susceptibility as a probe of low-frequency magnetic dynamics,” *J. Phys. Condens. Matter* **31**, 013001 (2019).
- ⁴⁴ P. Schiffer, A. P. Ramirez, D. A. Huse, P. L. Gammel, U. Yaron, D. J. Bishop, and A. J. Valentino, “Frustration Induced Spin Freezing in a Site-Ordered magnet: Gadolinium Gallium Garnet,” *Phys. Rev. Lett.* **74**, 2379 (1995).
- ⁴⁵ S. Shtrikman and E.P. Wohlfarth, “The theory of the Vogel-Fulcher law of spin glasses,” *Physics Letters A* **85**, 467–470 (1981).
- ⁴⁶ J. Mydosh, *Spin Glasses: An Experimental Introduction (1st ed.)* (CRC Press, 1993) <https://doi.org/10.1201/9781482295191>.
- ⁴⁷ O. Cépas and B. Canals, “Heterogeneous freezing in a geometrically frustrated spin model without disorder: Spontaneous generation of two time scales,” *Phys. Rev. B* **86**, 024434 (2012).
- ⁴⁸ P. Beauvillain, C. Dupas, J. P. Renard, and P. Veillet, “Experimental study of the spin freezing in an insulating spin-glass: Static and dynamical aspects,” *Phys. Rev. B* **29**, 4086 (1984).

Appendix A: Analysis of backscattering data

The Lorentzian signal sits atop a linear background, with the flat part $C_1(Q, T)$, increasing with temperature as shown in Fig. 12(a). The slope of the background depends slightly on Q and shows no systematic temperature dependence. Importantly, the slope is small compared with the flat part, and we can ignore it in the following analysis. The flat part of the background signal depends on temperature and Q , but can be subdivided into two parts to represent a background contribution from sample environment (T -independent part ($C_{\text{env}}(Q)$)) and a magnetic contribution, (Q -independent part, $C_{\text{mag}}(T)$):

$$C_1(Q, T) = C_{\text{env}}(Q) + C_{\text{mag}}(T). \quad (\text{A1})$$

Fig. 12(b) shows $C_{\text{mag}}(T)$, the magnetic component.

$C_{\text{mag}}(T)$ increases with increasing temperature and thus indicates that it originates from motions on a larger energy scale than the accessible energy window of IN16b

($\sim \pm 30 \mu\text{eV}$), similar to previous backscattering measurements on $\text{Tb}_2\text{Sn}_2\text{O}_7$ ⁴⁰. It is likely that this contribution originates from the tails of the lowest excitation, INS1, observed at 0.05(1) meV.

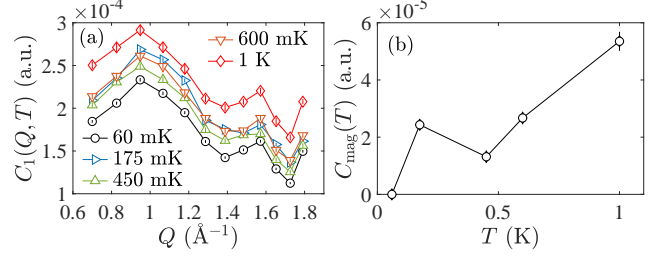


Figure 12. The flat background signal of GGG measured at IN16b. (a) shows the full signal, (b) shows the magnetic signal, $C_{\text{mag}}(T)$.